Collapse of electrons to a donor cluster in SrTiO_{3}

Han Fu, K. V. Reich, and B. I. Shklovskii

Phys. Rev. B **92**, 035204 — Published 10 July 2015

DOI: 10.1103/PhysRevB.92.035204

Collapse of electrons to a donor cluster in $SrTiO_3$

Han Fu,[1] K. V. Reich,[1,2,*] and B. I. Shklovskii[1]

[1] *Fine Theoretical Physics Institute, University of Minnesota, Minneapolis, MN 55455, USA*
[2] *Ioffe Institute, St Petersburg, 194021, Russia*

(Dated: June 24, 2015)

It is known that a nucleus with charge Ze, where $Z > 170$ creates electron-positron pairs from the vacuum. Electrons collapse onto the nucleus resulting in a net charge $Z_n < Z$ while the positrons are emitted. This effect is due to the relativistic dispersion law. The same reason leads to the collapse of electrons to the donor cluster with a large charge number Z in narrow-band gap semiconductors, Weyl semimetals and graphene. In this paper, a similar effect of electron collapse and charge renormalization is found for a donor cluster in $SrTiO_3$ (STO), but with a different origin. At low temperatures, STO has an enormously large dielectric constant and the nonlinear dielectric response becomes dominant when the electric field is still small. This leads to the collapse of electrons into a charged spherical donor cluster with radius R when its total charge number Z exceeds a critical value $Z_c \simeq R/a$ where a is the lattice constant. The net charge $Z_n e$ grows with Z until Z exceeds $Z^* \simeq (R/a)^{9/7}$. After this point, the charge of the compact core Z_n remains $\simeq Z^*$, while the rest Z^* electrons form a sparse Thomas-Fermi electron atmosphere around it. We show that the thermal ionization of such two-scale atoms easily strips the outer atmosphere while the inner core remains preserved. We extend our results to the case of long cylindrical clusters. We discuss how our predictions can be tested by measuring conductivity of chain of discs of charge on the STO surface.

I. INTRODUCTION

Recently, studies of ABO_3 perovskite crystals have been a subject of interest due to their intriguing magnetic, superconducting, and multiferroic properties[1] and subsequent significant technological applications. Among them, $SrTiO_3$ (STO) has attracted special attention[2,3]. STO is a semiconductor with a band gap of $\simeq 3.2$ eV and a large dielectric constant $\kappa = 2 \times 10^4$ at liquid helium temperature. Like the conventional semiconductors, STO can be used as the basis for a number of devices[4,5].

Many of the devices are realized by doping the bulk STO such as the reduction of STO through generating oxygen vacancies at high temperatures. The vacancies either form along a network of extended defects[6] or assemble together to lower the system's energy[7,8], probably producing large positively charged donor clusters. Another way to more controllably create such a cluster is to "draw" a disc of charge by the atomic force microscope (AFM) tip on the surface of LAO/STO structure with the subcritical thickness for $LaAlO_3$ (LAO)[9,10]. The potential caused by such a positive disc in the bulk STO is similar to that of a charged sphere.

Let's consider a spherical donor cluster with radius R and charge Ze. We assume that the cluster is located on the background of uniformly n-type doped STO in which the Fermi level is very close to the bottom of the conduction band. There are Z electrons located at distances from $\kappa b/Z$ to the Bohr radius κb from the cluster, which form a Thomas-Fermi "atom"[11] with it. Here $b = \hbar^2/m^* e^2$, $m^* \approx 1.8 m_e$ is the effective electron mass in STO[12] with m_e being the electron mass. Since κ is large, the electrons are far away from the cluster and the whole "atom" is very big. As Z increases, the electron gas swells inward to hold more electrons. However, we find that when Z goes beyond a certain value Z_c ($\kappa b/Z$ is still much larger than R at this moment), the physical picture is qualitatively altered. Surrounding electrons start to collapse into the cluster and the net cluster charge gets renormalized from Ze to $Z_n e$ with $Z_n \ll Z$ at very large Z.

The effect of charge renormalization is not new[13,14]. For a highly charged nucleus with charge Ze, the vacuum is predicted to be unstable against creation of electron-positron pairs, resulting in a collapse of electrons onto the nucleus with positrons emitted[13]. This instability happens when $Z > Z_c$ with $Z_c \simeq 170 \gtrsim 1/\alpha$, where $\alpha = e^2/\hbar c \simeq 1/137$ is the fine structure constant. When Z exceeds $Z^* \simeq 1/\alpha^{3/2} \simeq 137^{3/2}$, the net charge saturates at Z^*[14]. In the condensed matter setting, there are similar phenomena in narrow-band gap semiconductors and Weyl semimetals[14] as well as graphene[15]. In all these cases, the collapse happens because the energy dispersion of electrons is relativistic in the Coulomb field of a compact donor cluster playing the role of a nucleus. In our work, however, the collapse originates from the strong nonlinearity of dielectric constant in STO at small distances from the cluster. In the case of a spherical donor cluster, this nonlinearity leads to the change of the attractive potential near the cluster from being $\propto 1/r$ to $\propto 1/r^5$, resulting in the collapse of electrons to the cluster.

The phenomena of electron collapse and charge renormalization in both heavy nuclei and our work are presented in Fig. 1. In our case, the first electron collapses at $Z \simeq Z_c \simeq R/a$, where a is the lattice constant, and at $Z \gg Z^* \simeq (R/a)^{9/7}$, the net charge of nucleus $Z_n e$ saturates as $Z_n \simeq Z^*$.

In the remainder of this paper, we use the Thomas-Fermi approximation to show how the electron gas col-

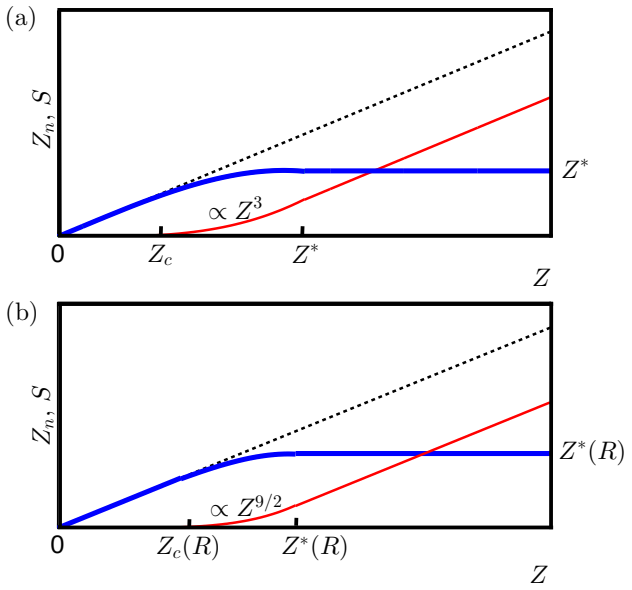

FIG. 1. (Color online) The number of collapsed electrons S and the renormalized net charge $Z_n e$ as a function of the original charge Ze. S is shown by the thin solid line (red), Z_n is denoted by the thick solid line (blue), and the dashed line (black) is a guide-to-eye where $Z_n = Z$. Z_c denotes the critical value where electrons begin to collapse and Z^* is the saturation point where Z_n stops growing. (a) Collapse of electrons and charge renormalization for highly charged nuclei. $S \propto Z^3$ at $Z_c \ll Z \ll Z^*$[16]. (b) Collapse of electrons and charge renormalization for spherical donor clusters in STO. $S \propto Z^{9/2}$ at $Z_c \ll Z \ll Z^*$.

lapses into the cluster at $Z \gg Z_c$ and find the corresponding electron density. In Sec. II, we demonstrate that when $Z_c \ll Z \ll Z^*$, the charge renormalization is relatively weak and the final charge number Z_n is just a little bit below Z. On the other hand, when $Z \gg Z^*$, the renormalization is very strong and Z_n is maintained at the level of Z^*. The inner core of the cluster atom with charge Z^* is surrounded by a sparse Thomas-Fermi atmosphere of Z^* electrons in which the large linear dielectric constant plays the main role. In Sec. III, we generalize our studies to the cylindrical donor clusters and introduce the notion of maximum linear charge density $\eta*$ similar to Z^* which is got when the bare charge density of the cluster η is large. In Sec. IV we consider the thermal ionization of donor cluster atoms and arrive at the conclusion that for both spheres and cylinders the external electron atmosphere is easily ionized while the inner core with charge Z^* or linear charge density $\eta*$ is robust against the ionization. We suggest experimental verification of our theory for a periodic chain of charge discs created by methods of Ref. 9 and 10. If neighboring disc atoms overlap via the outer electron atmosphere (the "bridges"), raising temperature may ionize these bridges and sharply reduce the chain conductance. We conclude our work in Sec. V.

II. SPHERICAL DONOR CLUSTERS

A. Nonlinear Dielectric Response

It is well known that STO is a quantum paraelectric where the onset of ferroelectric order is suppressed by quantum fluctuations[17]. In such ferroelectric-like materials, the free energy density F can be expressed by the Landau-Ginzburg theory as a power-series expansion of the polarization P[18]:

$$F = F_0 + \frac{\tau}{2}P^2 + \frac{A}{4P_0^2}P^4 - EP$$

(in Gaussian units), where F_0 stands for the free energy density at $P = 0$, E is the electric field, $\tau = 4\pi/(\kappa - 1) \simeq 4\pi/\kappa$ is the inverse susceptibility, $\kappa \gg 1$ is the dielectric constant, $A \approx 0.9$[19], $P_0 = e/a^2$, $a = 3.9\,\mathring{A}$ is the lattice constant. We neglect the gradient terms of polarization since they play a minor role in the nonlinear regime. We assume that the dielectric response is isotropic. This is justified by the small anisotropy in the nonlinear response of STO[20]. The crystal polarization P is determined by minimizing the free energy density F in the presence of the electric field E, i.e., $\delta F/\delta P = 0$. This gives

$$E = \frac{4\pi P}{\kappa} + \frac{AP^3}{P_0^2}.$$

For very big κ, the nonlinear term in this expression is likely to dominate over the linear one even at relatively small P as long as $P \gg \sqrt{4\pi/\kappa A}P_0$. At distances not too far from the cluster, this relationship can easily be satisfied and the dielectric response becomes nonlinear[19]:

$$E = \frac{AP^3}{P_0^2}. \tag{1}$$

Since $P_0 = e/a^2$ is really big, we can expect that $P < \sqrt{4\pi/A}P_0$ always holds, which gives $E < 4\pi P$. Then,

$$D = E + 4\pi P \approx 4\pi P. \tag{2}$$

According to the Gauss's law in dielectric media, we know $\nabla \cdot D = 4\pi\rho$ where ρ is the free charge density. Together with Eqs. (1) and (2), we have

$$\nabla \cdot (\nabla\phi)^{1/3} = -\left(\frac{A}{P_0^2}\right)^{1/3}\rho \tag{3}$$

where ϕ is the electric potential.

Below, we show that this nonlinear dielectric response leads to the collapse of electrons into the spherical donor cluster inside STO when the cluster charge is large enough.

B. Renormalization of Charge

Consider a large spherical donor cluster of the radius R and the total positive charge Ze such that $a \ll R <$

$\kappa b/Z$. If the dielectric response is linear, the electrons are mainly located at distances between $r_1 = \kappa b/Z$ and $r_A = \kappa b$ from the cluster[11] where $b = \hbar^2/m^*e^2 \approx 0.29\,\mathring{A}$[19]. For a very large κ, these radii are huge ($r_A = 700$ nm in STO at liquid helium temperature where $\kappa = 20000$) and the electrons are far away from the cluster. However, at small distances, the dielectric response is nonlinear and changes the potential form. If the potential energy outweighs the kinetic energy, electrons are attracted to the cluster and renormalize the net charge. To see when this will happen, we look at the specific form of electric potential in this situation. We can calculate the potential from Eq. (3). But due to the simple charge distribution here, we can get it in an easier way. At $r > R$ where r is the distance from the cluster center, the sphere looks like a point charge and $D(r) = Ze/r^2$. Using this together with Eqs. (1) and (2), one can calculate the electric field and get the electric potential $\phi(r)$ as:

$$\phi(r) = \frac{A}{P_0^2}\left(\frac{Ze}{4\pi}\right)^3 \frac{1}{5r^5}, \qquad R < r \ll r_1 \quad (4)$$

with $\phi(r = \infty)$ defined as zero. Inside the cluster at $r < R$, since the charge is uniformly distributed over the sphere, the total positive charge enclosed in the sphere of radius r is equal to Zer^3/R^3, so $D(r) = Zer/R^3$. One then gets the corresponding potential $\phi(r)$:

$$\phi(r) = \frac{A}{P_0^2}\left(\frac{Ze}{4\pi}\right)^3 \left(\frac{9}{20}\frac{1}{R^5} - \frac{1}{4}\frac{r^4}{R^9}\right), 0 < r < R \quad (5)$$

using the boundary condition $\phi(r = R^-) = \phi(r = R^+)$. A schematic graph of the potential energy $U(r) = -e\phi(r)$ is shown in Fig. 2 by the thick solid line (blue).

The Hamiltonian for a single electron is $H = p^2/2m^* - e\phi(r)$, where p is the momentum of the electron and m^* is the effective electron mass in STO[19]. If we approximately set $p \simeq \hbar/2r$, we get a positive total energy of the electron everywhere when Z is very small. This means there are no bound states of electron in the cluster. However, when Z is big enough so that $Z > Z_c$, the electron can have negative total energy at $r < R$ and will collapse into the cluster. Using Eqs. (4) and (5), we find

$$Z_c \approx \frac{4\pi(b/Aa)^{1/3}R}{a} \sim \frac{R}{a} \gg 1. \quad (6)$$

As Z continues increasing, more and more electrons get inside the cluster filling it from the center where the potential energy is lowest (see Fig. 2). The single-electron picture no longer applies. Instead, we use the Thomas-Fermi approximation[11] with the electrochemical potential $\mu = 0$, which gives:

$$n(r) = \frac{c_1}{b^3}\left[\frac{\phi(r)}{e/b}\right]^{3/2}, \quad (7)$$

where $n(r)$ is the electron density at radius r, $c_1 = 2^{3/2}/3\pi^2 \approx 0.1$.

We assume that the bulk STO is a heavily doped semiconductor in which the Fermi level lies in the conduction band. On the other hand, due to the relatively high effective electron mass, the Fermi energy is much smaller than the depth of the potential well shown in Fig. 2 and is thus ignored. Since at $r = \infty$ the electric potential $\phi(r)$ is defined as 0, we then have the electrochemical potential $\mu \simeq 0$.

When the number of collapsed electrons S is small, their influence on the electric potential is weak. One can still use Eqs. (4) and (5) for $\phi(r)$ and get the corresponding expression of $n(r)$. At $r > R$, since $\phi(r)$ is $\propto 1/r^5$, we get $n(r) \propto 1/r^{15/2}$. In this way, we calculate S as

$$S = \int_0^\infty n(r)4\pi r^2 dr = 0.5Z\left(\frac{Z}{Z^*}\right)^{7/2} \propto Z^{9/2}, \quad (8)$$

where

$$Z^* = \left[\frac{4\pi(b/Aa)^{1/3}R}{a}\right]^{9/7}, \quad (9)$$

The net charge number of the cluster is

$$Z_n = Z - S = Z\left[1 - 0.5\left(\frac{Z}{Z^*}\right)^{7/2}\right]. \quad (10)$$

One can see, when $Z_c \ll Z \ll Z^*$, one gets $S \ll Z$ and $Z_n \lesssim Z$, meaning the charge renormalization is weak. However, at $Z \sim Z^*$, according to Eqs. (8) and (10), we get $Z_n \sim S \sim Z^*$. The potential contributed by electrons is no longer perturbative. This brings us to the new regime of strong renormalization of charge.

We show that at $Z \gg Z^*$ the net charge $Z_n e$ saturates at the level of Z^*e. Indeed, when Z grows beyond Z^*, Z_n can not go down and therefore can't be much smaller than Z^*. At the same time it can not continue going up, otherwise as follows from Eqs. (4) and (8) with Z replaced by $Z_n \gg Z^*$, the total electron charge surrounding the charge $Z_n e$ at $r > R$ would become $Se \simeq Z_n e(Z_n/Z^*)^{7/2} \gg Z_n e$ leading to a negative charge seen from infinity. Thus, at $Z \gg Z^*$, the net charge Z_n saturates at the universal value of the order of Z^* as is shown in Fig. 1b. As we emphasized in Fig. 1, this result is qualitatively similar to the one obtained for heavy nuclei and donor clusters in Weyl semimetals and narrow-band gap semiconductors in Ref. 14.

In the following subsection, we show how the renormalization of charge at $Z \gg Z^*$ is realized through certain distribution of electrons, in which a structure of "double layer" (see Fig. 2) plays an important role.

C. Radial Distribution of Electrons

At $Z \gg Z^*$, the charge renormalization is strong and the most of the sphere of radius R is completely neutralized by electrons. In the neutral center of the sphere,

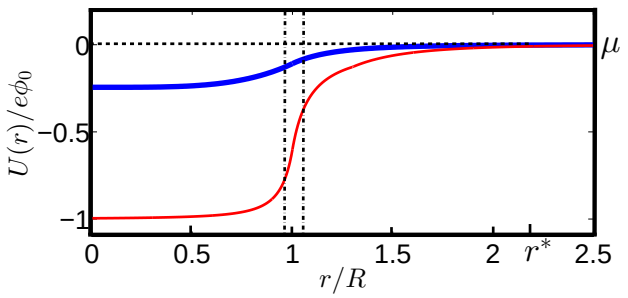

FIG. 2. (Color online) Potential energy of electrons $U(r) = -e\phi(r)$ as a function of radius r. ϕ_0 is defined as $n(\phi_0) = n_0$, where $n_0 = 3Z/4\pi R^3$, $n(r)$ is a function of $\phi(r)$ given by Eq. (7). The thick solid line (blue) represents the potential profile of a cluster of charge $Z \lesssim Z^*$ which is in the regime of weak charge renormalization. The thin solid line (red) represents the potential of a cluster at $Z \gg Z^*$ in the strong renormalization regime, where the two vertical dotted lines show edges of the "double-layer" structure of width $\sim d \ll R$. The horizontal dashed line (black) indicates the position of the chemical potential $\mu = 0$. r^* is the external radius of the collapsed electron gas where Thomas-Fermi approach fails.

the electron density $n(r) = n_0$, where $n_0 = 3Z/4\pi R^3$ is the density of the positive charge inside the cluster. The corresponding "internal" electric potential $\phi_{in}(r) = \phi_0$ where ϕ_0 is given by $n(\phi_0) = n_0$ using Eq. (7). $\phi_{in}(r)$ is then $\propto (n_0 a^3)^{2/3} \propto [Z/(R/a)^3]^{2/3}$. Outside the cluster, when the charge is renormalized to Z_n, one gets a potential $\phi_{out}(r)$ similar to Eq. (4) with Z replaced by Z_n. Since Z_n is $\sim Z^*$ where Z^* is given by Eq. (9), we get $\phi_{out}(r) \propto (R/a)^{-8/7}$ at a distance r of the order R. Thus, close to the cluster surface, the ratio of the outside potential $\phi_{out}(r)$ to the inside potential $\phi_{in}(r)$ is $\simeq (R/a)^{6/7}/Z^{2/3} \ll 1$ since $Z \gg Z^* \simeq (R/a)^{9/7}$. This indicates a sharp potential drop across the sphere surface.

At $0 < R - r \ll R$, there's a thin layer of uncompensated positive charges. At $0 < r - R \ll R$, a higher potential than farther away means a larger electron concentration that forms a negative layer close to the surface. This "double-layer" structure resembles a capacitor which quickly brings the potential down across the surface as shown in Fig. 2. An analogous structure also exists in heavy nuclei[13,16] with charge $Z \gg 1/\alpha^{3/2}$.

To make the analysis more quantitative, one needs to know the specific potential profile in this region. Using Eq. (3), we get the general equation of $\phi(r)$ in the spherical coordinate system:

$$\left(\frac{d}{dr} + \frac{2}{r}\right)\left(\frac{d\phi}{dr}\right)^{1/3} = \frac{A^{1/3}e}{P_0^{2/3}}\left[n(r) - n_0\right], \; r < R \quad \text{(11a)}$$

$$\left(\frac{d}{dr} + \frac{2}{r}\right)\left(\frac{d\phi}{dr}\right)^{1/3} = \frac{A^{1/3}e}{P_0^{2/3}} n(r), \qquad r > R \quad \text{(11b)}$$

Near the cluster surface, we can approximately use a plane solution of $\phi(r)$, i.e., ignore the $2/r$ term on the left side. This kind of solution for $r \gtrsim R$ is already known[19]:

$$\phi(r) = \frac{c_3}{A^{2/7}}\frac{e}{b}\left(\frac{b}{a}\right)^{16/7}\left(\frac{a}{x+d}\right)^{8/7}, \qquad (12)$$

where $x = r - R \ll R$ is the distance to the surface and $d \ll R$ is the characteristic decay length to be determined, $c_3 \approx 6$. Correspondingly, the radial electron concentration at $r \gtrsim R$ is given by

$$\begin{aligned} n(r)r^2 &= \frac{c_4}{A^{3/7}}\frac{1}{b^3}\left(\frac{b}{a}\right)^{24/7}\left(\frac{a}{x+d}\right)^{12/7} r^2 \\ &\approx \frac{c_4}{A^{3/7}}\frac{1}{b^3}\left(\frac{b}{a}\right)^{24/7}\left(\frac{a}{x+d}\right)^{12/7} R^2, \end{aligned} \qquad (13)$$

where $r \approx R$, $c_4 \approx 1$.

Since the "double-layer" structure resembles a plane capacitor, near the surface, the potential drop is nearly linear with the radius. Using Eq. (12), one can get $\phi(r) \approx (1 - 8x/7d)\phi(R)$ at $0 < x = r - R \ll d$, which gives the electric field $8\phi(R)/7d$ inside the "double layer". At $r < R$, this electric field persists and gives $\phi(r) \approx (1 + 8x/7d)\phi(R)$ at $0 < x = R - r \ll d$. As r further decreases, the positive layer ends and the potential crosses over to the constant value ϕ_0 given by $n(\phi_0) = n_0$ using Eq. (7). This boundary condition gives

$$d = \frac{c_5}{A^{1/4}}\left(\frac{b}{a}\right)^{1/4}\frac{a}{(n_0 a^3)^{7/12}}, \qquad (14)$$

where $c_5 \approx 2$. By expressing n_0 in terms of Z and R, we get $d/R \propto (Z^*/Z)^{7/12} \ll 1$ at $Z \gg Z^*$.

According to Eq. (12), when x is comparable to R and the plane approximation is about to lose its validity, $\phi(r)$ is $\propto (R/a)^{-8/7}$. It is weak enough to match the low electric potential $\phi_{out}(r) \propto (R/a)^{-8/7}$ caused by the renormalized charge $Z_n \sim Z^*$ at $r \sim R$. The plane solution then crosses over to the potential $\phi_{out}(r) \propto Z^{*3}/r^5$ which is the asymptotic form at large distances.

A schematic plot of the potential energy $U(r) = -e\phi(r)$ as a function of radius r is shown in Fig. 2 by the thin solid line (red). The corresponding radial distribution of electrons is shown in Fig. 3 by the thick solid line (red).

So far, we have got a $1/r^5$ potential $\phi(r)$ and $1/r^{11/2}$ radial electron concentration $n(r)r^2$ at $r \gg R$ in both weak and strong charge renormalization cases. However, as the electron density decreases to certain extent so that the Fermi wavelength λ is comparable to the radius r, the gas is no longer degenerate and the Thomas-Fermi approach fails. Since $\lambda \simeq n(r)^{-1/3}$, we get this radius $r^* \simeq Z^* a$ at $Z \gg Z^*$. One should then return to the Schrodinger equation used for a single electron. Since the uncertainty principle estimates that the kinetic energy decays as $1/r^2$ while the potential energy is $\propto -Z^{*3}/r^5$, the potential energy is smaller than the kinetic energy in magnitude at $r > r^*$, which means electrons can not stay

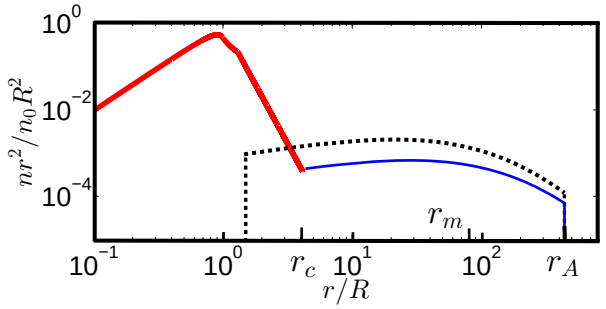

FIG. 3. (Color online) Radial electron concentration $n(r)r^2$ as a function of radius r. The thick solid line (red) represents the inner collapsed electrons at $r < r_c$ where the dielectric response is nonlinear. The thin solid line (blue) shows the electrons belonging to the outer shell which form the standard Thomas-Fermi atom with the renormalized nucleus of charge Z^* at $r > r_c$, where the dielectric response is linear. This electron gas ends at the Bohr radius $r_A = \kappa b$ while most of them are at radius $r_m = \kappa b/Z^{*1/3}$. The dashed line (black) denotes the electrons forming a Thomas-Fermi atom[11] with a nucleus of charge Z when P_0 is infinity and there's no range with nonlinear dielectric response. The reduction of electron density in the outer shell of electrons due to the collapse is substantial. The reason this is not immediately seen from the difference of height between the dashed line (black) and the thin solid line (blue) is that we use a logarithmic scale here. n_0 is defined as $3Z/4\pi R^3$. This graph is plotted at $b = 0.35\,\mathring{A}$, $a = 3.9\,\mathring{A}$, $A = 0.9$, $R = 4.4a$, $\kappa = 20000$, $n_0 = 0.8/a^3$.

at radii larger than r^*. One can also find that using the Thomas-Fermi solution $\phi_{out}(r)$, the total electron number calculated at $r > r^*$ is ~ 1, which again indicates there's no electron at $r > r^*$ considering the discreteness of electron charge. As a result, the $1/r^{11/2}$ tail of radial electron concentration will not continue to infinity but stop at radius r^*. This is a semi-classical result. Quantum mechanical analysis shows that the electron density does not go to zero right at r^* but decays exponentially after this point. Since this decay is fast and brings very small corrections to the end of the inner electron gas, we don't consider it here.

At $\kappa = \infty$, the rest of the electrons are at the infinity so that we are dealing with a positive ion with charge Z^*. At finite but very large κ, at certain distance from the cluster, the field is so small that $P > \sqrt{4\pi/\kappa A}P_0$ is no longer satisfied and the linear dielectric response is recovered. Things then become quite familiar. Electrons are mainly located between $r_1 = \kappa b/Z^*$ and $r_A = \kappa b$ with the majority at radius $r_m = \kappa b/Z^{*1/3}$ as given by the Thomas-Fermi model[11]. Although quantum mechanics gives a nonzero electron density at $r < r_1$, the number of total electrons within this radius is only ~ 1 and can be ignored. So approximately, when $r_1 \gg r^*$, i.e., $\kappa \gg (Z^*)^2 \simeq (R/a)^{18/7}$, there's a spatial separation between inner collapsed electrons and outer ones that form the usual Thomas-Fermi atom with the renormalized nucleus. When κ is not so big, such separation is absent, which actually happens more often in real situations. The inner tail then connects to the outer electrons with the Thomas-Fermi approach valid all the way and the dielectric response becomes linear at $r = r_c \propto a\kappa^{1/4}Z^{*1/2}$. One should note, as long as κ is large enough to satisfy $r_m \gg R$ which gives $\kappa \gg (R/a)^{10/7}$, the majority of the outer electrons located at r_m haven't intruded into the cluster or the highly screening double-layer structure near the cluster surface. The charge renormalization process remains undisturbed and the total net charge seen by outer electrons is still Z^*. The corresponding radial electron concentration $n(r)r^2$ is shown in Fig. 3. At $\kappa \ll (R/a)^{10/7}$, in most of the space the dielectric response is linear. In that case, almost all electrons reside in the cluster with only some spill-over near the surface. The positive and negative charges are uniformly distributed inside the cluster as described by the Thompson "jelly" model.

III. CYLINDRICAL DONOR CLUSTERS

In some cases, the donor clusters are more like long cylinders than spheres. For this situation, a cluster is described by the linear charge density ηe while its radius is still denoted as R. We use a cylindrical coordinate system with the z axis along the axis of the cylinder cluster and r as the distance from the axis. We show that when the charge density ηe is larger than certain value $\eta_c e$, electrons begin to collapse into the cluster and the charge density is weakly renormalized. When η exceeds another value $\eta^* \gg \eta_c$, the renormalization becomes so strong that the net density η_n remains $\simeq \eta^*$ regardless of the original density η (see Fig. 4). Our problem is similar to that of the charged vacuum condensate near superconducting cosmic strings[21], and is also reminiscent of the Onsager-Manning condensation[22] in salty water[23].

Renormalization of Linear Charge Density.— For a uniformly charged cylindrical cluster with a linear charge density ηe, similar to what we did in Sec. II, we get $D(r) = 2\eta(r)e/r$, where $\eta(r) = \eta r^2/R^2$ at $r < R$ and $\eta(r) = \eta$ at $r > R$. We then can calculate the electric field using Eqs. (1) and (2) and get the electric potential $\phi(r)$ as:

$$\phi(r) = \frac{A}{P_0^2}\left(\frac{\eta e}{2\pi}\right)^3\left(\frac{3}{4}\frac{1}{R^2} - \frac{1}{4}\frac{r^4}{R^6}\right), 0 < r < R \quad \text{(15a)}$$

$$\phi(r) = \frac{A}{P_0^2}\left(\frac{\eta e}{2\pi}\right)^3\frac{1}{2r^2}, \qquad R < r \quad \text{(15b)}$$

with $\phi(r = \infty)$ chosen to be 0. The corresponding potential energy $U(r) = -e\phi(r)$ is shown in Fig. 5 by the thick solid line (blue). Using the Schrodinger equation and setting the momentum $p \simeq \hbar/2r$, we find that the tightly bound states of electrons, in which electrons are strongly confined within the cluster (at $r < R$), exist only

when $\eta > \eta_c$ where

$$\eta_c \approx 2\pi \left(\frac{b}{Aa}\right)^{1/3} \frac{1}{a}, \tag{16}$$

which, contrary to the Z_c value got in the spherical case, does not depend on R. Electrons begin to collapse into the cluster at $\eta > \eta_c$ and in the beginning they are located near the axis where the potential energy is lowest (see Fig. 5). With increasing η, the electron density grows and one can adopt the Thomas-Fermi description. Using Eq. (7) and (15b), one gets the electron density $n(r) \propto 1/r^3$ at $r > R$ and the total number of collapsed electron per unit length is

$$\theta = \int_0^\infty n(r) 2\pi r dr = 0.5\eta \left(\frac{\eta}{\eta^*}\right)^{7/2} \propto \eta^{9/2}, \tag{17}$$

where

$$\eta^* = \frac{1}{a}\left[2\pi \left(\frac{b}{Aa}\right)^{1/3}\right]^{9/7} \left(\frac{R}{a}\right)^{2/7}. \tag{18}$$

The net charge density $\eta_n e$ is then renormalized to

$$\eta_n = \eta - \theta = \eta\left[1 - 0.5\left(\frac{\eta}{\eta^*}\right)^{7/2}\right]. \tag{19}$$

At $\eta \ll \eta^*$, the renormalization of charge density is weak and η_n grows with η. At $\eta > \eta^*$, the number of collapsed electrons is large and the renormalization effect is strong. Most of the cluster is then neutralized by electrons and the final net density η_n is much smaller than η. Following the logics similar to those in the spherical case, and by using Eq. (17), one can show that η_n reaches a saturation value of η^* at $\eta \gg \eta^*$. The dependence of η_n on η is shown in Fig. 4, which resembles Fig. 1.

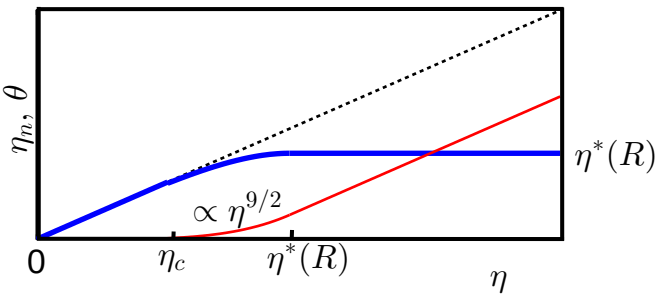

FIG. 4. (Color online) Number of collapsed electrons per unit length θ and renormalized net charge density η_n as a function of cluster charge density η. The thick solid line (blue) shows $\eta_n(\eta)$. The thin solid line (red) represents $\theta(\eta)$. The dashed line (black) is a guide-to-eye with $\eta_n = \eta$. $\theta(\eta) \propto \eta^{9/2}$ at $\eta_c \ll \eta \ll \eta^*$.

Radial Distribution of Electrons.— At $\eta \gg \eta^*$, there are lots of collapsed electrons inside the cluster where $n(r) = n_0 = \eta/\pi R^2$ and the potential energy is low. Again, there's a "double-layer" structure on the surface that provides steep growth of potential energy with r at $r = R$. Close to the cylinder surface at $0 < r - R \ll R$, as for the sphere, we can approximately use a plane solution of $\phi(r)$ as given by Eq. (12). The expression of the characteristic decay length d is also the same as in Eq. (14). When $x = r - R$ is comparable to R, the plane solution crosses over to the fast decaying potential $\propto 1/r^2$ as given by Eq. (15b) with η replaced by $\eta_n \simeq \eta^*$. A schematic plot of the potential energy $U(r) = -e\phi(r)$ is shown in Fig. 5.

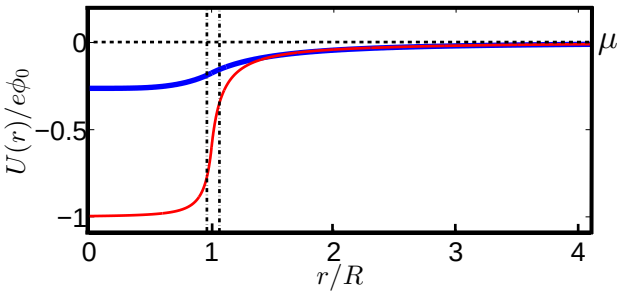

FIG. 5. (Color online) Potential energy of electrons $U(r) = -e\phi(r)$ as a function of radius r. ϕ_0 is defined as $n(\phi_0) = n_0$, where $n_0 = \eta/\pi R^2$, $n(r)$ is a function of $\phi(r)$ given by Eq. (7). The thick solid line (blue) represents the potential profile of a cluster of charge density $\eta \lesssim \eta^*$ which is in the regime of weak renormalization of charge. The thin solid line (red) represents the potential of a cluster with $\eta \gg \eta^*$ which is in the strong renormalization regime. The two vertical dotted lines show edges of the "double-layer" structure of width $\sim d \ll R$. The horizontal dashed line (black) indicates the position of the chemical potential $\mu = 0$.

This potential produces a universal tail of electron density $n(r) \sim 1/r^3$. The corresponding radial electron concentration $n(r)r$ is $\sim 1/r^2$. Since the Fermi wavelength $\lambda \simeq n(r)^{-1/3}$, we get $\lambda \sim r$, i.e., the Thomas-Fermi approach is only marginally valid. The collapsed electrons extend until the linear dielectric response is recovered and then connect to the outer electrons.

IV. FINITE-TEMPERATURE IONIZATION OF CLUSTER ATOMS AND ITS EXPERIMENTAL IMPLICATIONS.

So far, we dealt with very low temperature. At a finite temperature T, the neutral cluster atom can get ionized due to the entropy gain of ionized electrons. The donor cluster atom becomes a positive ion with charge $Z_i(T)e$. Our goal below is to find this charge.

We assume that we have a small but finite three-dimensional concentration N of spherical clusters and the charge $Z_i(T) < Z^*$, i. e., the outer electron shell is still incompletely ionized. Such a cluster can bind electrons with an ionization energy $Z_i(T)^2 e^2/\kappa^2 b$. We

can find $Z_i(T)$ by equating this energy with the decrease in the free energy per electron $k_BT\ln(n_0/n)$ due to the entropy increase, where k_B is the Boltzmann constant, $n = Z_i(T)N$ is the concentration of ionized electrons and $n_0 = 2/\lambda^3$ with $\lambda = \sqrt{2\pi\hbar^2/m^*k_BT}$ as the De-Broglie wavelength of free electrons at temperature T. At $\kappa = 20000$, $b = 0.29\,\mathring{A}$, $m^* = 1.8m_e$ where m_e is the electron mass and $N = 10^{15}$ cm^{-3} (estimated from that the concentration of total donor electrons is around 10^{18} cm^{-3} and each cluster contributes ~ 300 donor electrons), we get $Z_i(T) \gtrsim Z^*$ at $T \gtrsim 8$ K with $Z^* = 100$ which is a reasonable estimate. This shows that the outer electrons are completely ionized at temperatures that are not too low. For the inner core electrons, the dielectric response is nonlinear and the attractive potential is stronger. So the ionization energy is higher $\simeq A(Z^*e/4\pi)^3/5P_0^2R^5$ for electrons at $r \simeq R$. At $R = 4a$, it is found that only at $T > 450$ K can the inner electrons be ionized by a considerable quantity (the $1/r^{15/2}$ tail is completely stripped then). So the inner electrons are robust against the thermal ionization.

For the cylindrical cluster, since it can effectively be regarded as the assembly of sphere clusters, one can expect that electrons are harder to be stripped off than in the spherical case. The thermal ionization is thus somewhat weaker. For the outer electrons, the dielectric response is linear and the ionization degree is determined by the Onsager-Manning linear density η_{OM}[22]. It can be derived as follows. The potential energy of electrons caused by the cylindrical charge source with a linear density $\eta_i e$ grows with the radius r as $2\eta_i e^2\ln(r/r_0)/\kappa$ while the entropy increases as $2k_B\ln(r/r_0)$, where r_0 is a chosen reference point. In equilibrium, by equating the energy increase and the entropic decrease of the free energy one gets the critical concentration $\eta_i = \eta_{OM} = \kappa k_BT/e^2$. This is the universal value of the net charge density, which depends only on the temperature T and the dielectric constant κ of the media similar to the case of DNA in salty water[23].

When the outer electrons are completely ionized, the charge density is expected to be η^*e given by Eq. (18). Taking $R = 4a$, $A = 0.9$, $\kappa = 20000$, $a = 3.9\,\mathring{A}$ and $b = 0.29\,\mathring{A}$, we get $\eta_{OM} \gtrsim \eta^*$ at $T \gtrsim 10$ K. Thus, the ionization of the outer shell proceeds until T grows to 10 K. Since the product κT is almost fixed at $T > 10$ K, η_{OM} actually stops growing with the temperature at $T > 10$ K. This practically means that only outer electrons are ionized at $T > 10K$. The inner electrons are well preserved against the ionization even at $T > 10$ K.

Thus, in both spherical and cylindrical cases, the outer electrons are thermally ionized at not very low temperature while the inner ones are mainly kept by the cluster. The final observable charge or charge density is then equal to Z^* or η^*. Below we will discuss how one can observe the thermal ionization.

Experimentally, charged clusters can be created controllably on the surface of LAO/STO structure when the LAO layer is of subcritical thickness $\lesssim 3$ unit cell[9,10]. A conducting atomic force microscope (AFM) tip is placed in contact with the top $LaAlO_3$ (LAO) surface and biased at certain voltage with respect to the interface, which is held at electric ground. When the voltage is positive, a locally metallic interface is produced between LAO and STO where some positive charges are accumulated in the shape of a disc. The same writing process can also create a periodic array of charged discs.

Let's first concentrate on a disc of positive charge created in this manner on the STO surface. Close to the surface and in the bulk STO, one should apply the plane solution given by Ref. 19 and repeated by Eq. (12) above. When the distance r from the disc center is large, i.e., $r \gg R$, the disc behaves like a charged sphere. Our results for a sphere are still qualitatively correct in this case.

In a periodic array of highly charged discs with period $2L$ (see Fig. 3a in Ref. 9), the linear concentration of free electrons responsible for the conductance at a very low temperature is of the order of $n(L)L^2$, where $n(r)$ is the electron density around a spherical donor cluster given by Sec. II. When the overlapping parts between neighboring discs belong to the outer electron shells, the corresponding density at $r = L$ is that of a Thomas-Fermi atom with charge Z^*. In this situation, the overlapping external atmosphere forms conductive "bridges" between discs at low temperature. When T increases, however, the outer electrons are ionized and the bridges are gone. These free electrons spread out over the bulk STO. At $T \lesssim 30$ K, electrons are scattered mainly by the Coulomb potential of donors and the corresponding mobility decreases with a decreased electron velocity. For the electrons ionized into the vast region of the bulk STO, they're no longer degenerate, so their velocity becomes much smaller at relatively low temperature. This results in a much smaller mobility of the ionized electrons than those bound along the chain. Their contribution to the conductivity is thus negligible. The system becomes more resistive due to the ionization and one can observe a sharp decrease of the conductivity along the chain. It may be possible for the chain to transition from a conducting "line" to multi-quantum-dots. Interesting phenomena of the conductance behavior such as the Coulomb blockade can probably emerge.

V. CONCLUSION

In this paper we have studied the structure of a many-electron "atom" whose center is a strongly charged donor cluster. It is determined by the collapse of electrons to the cluster in $SrTiO_3$ due to the nonlinear dielectric response at small distances from the cluster surface. For a spherical cluster, when its charge number exceeds a critical value Z_c, the potential well inside it becomes deep enough to trap electrons despite their high kinetic energy. In the beginning, the cluster charge Ze is weakly renormalized by the electrons. When Ze grows beyond

another value Z^*, the number of collapsed electrons becomes large so that the most of the cluster is neutralized and the charge is strongly renormalized to Z^*. This strong renormalization is realized via a "double-layer" structure on the cluster surface. The corresponding potential profiles and radial distributions of electrons are investigated. The critical and saturation values are found to be dependent only on the cluster radius: $Z_c \simeq (R/a)$ and $Z^* \simeq (R/a)^{9/7}$. At zero temperature, a renormalized cluster with charge Z^* is the nucleus of a Thomas-Fermi atom. This nucleus is surrounded by the external electron atmosphere which is sparse due to the weak Coulomb interaction at a large dielectric constant. These outer electrons can easily be stripped off by the thermal ionization leaving only the compact ionic core with charge Z^*. The case of a cylindrical donor cluster is discussed as well where similar results are found. Namely, when its linear charge density ηe is larger than $\eta_c e \simeq e/a$, electrons start collapsing to the cluster. At $\eta \gg \eta^*$ where $\eta^* \simeq (R/a)^{2/7}/a$ is the saturation density, the net charge density of the cluster $\eta_n e$ stays at the level of $\eta^* e$. At zero temperature, this renormalized cylindrical cluster is surrounded by a sparse electron atmosphere which can be ionized at temperatures larger than 10 K. We also discuss how one can verify our predictions by measuring the conductivity of a chain of charged discs on the surface of LAO/STO structures.

In this work, the mean-field Thomas-Fermi approach has been applied. It is simple yet has shown reasonable agreement with more exact calculations[24–29] in the planar STO model[19]. In that model, instead of constituting spherical or cylindrical dopant clusters inside STO, the electron-providing material such as LAO is outside the bulk STO and forms a planar interface with STO over which electrons spill out. The width of the electron distribution layer inside STO derived using the Thomas-Fermi approximation[19] is consistent with results got from ab initio calculations and other non-mean-field microscopic models[24–29]. Therefore, it is natural to expect that the Thomas-Fermi approach is a good approximation for different geometries (spherical and cylindrical) as well, since in this work we also deal with spatial scales larger than the lattice constant.

Acknowledgments.

We are grateful to B. Skinner, E. B. Kolomeisky, B. Jalan, C. Leighton, A. P. Levanyuk and J. Levy for careful reading of the manuscript and valuable advice, and to A. Kamenev, D. L. Maslov, A. Vainshtein and M. B. Voloshin for helpful discussions. This work was supported primarily by the National Science Foundation through the University of Minnesota MRSEC under Award No. DMR-1420013.

* Reich@mail.ioffe.ru

[1] J. Chakhalian, J. W. Freeland, A. J. Millis, C. Panagopoulos, and J. M. Rondinelli, Rev. Mod. Phys. **86**, 1189 (2014).
[2] S. Stemmer and S. J. Allen, Annual Review of Materials Research **44**, 151 (2014).
[3] P. Zubko, S. Gariglio, M. Gabay, P. Ghosez, and J.-M. Triscone, Annual Review of Condensed Matter Physics **2**, 141 (2011).
[4] A. Ohtomo and H. Y. Hwang, Nature **427**, 423 (2004).
[5] Y. Xie, C. Bell, Y. Hikita, S. Harashima, and H. Y. Hwang, Advanced Materials **25**, 4735 (2013).
[6] K. Szot, W. Speier, R. Carius, U. Zastrow, and W. Beyer, Phys. Rev. Lett **88**, 075508 (2002).
[7] D. D. Cuong, B. Lee, K. M. Choi, H.-S. Ahn, S. Han, and J. Lee, Phys. Rev. Lett **98**, 115503 (2007).
[8] D. A. Muller, N. Nakagawa, A. Ohtomo, J. L. Grazul, and H. Y. Hwang, Nature (London) **430**, 657 (2004).
[9] C. Cen, S. Thiel, G. Hammerl, C. W. Schneider, K. E. Andersen, C. S. Hellberg, J. Mannhart, and J. Levy, Nature Materials **7**, 298 (2008).
[10] F. Bi, D. F. Bogorin, C. Cen, C. W. Bark, J.-W. Park, C.-B. Eom, and J. Levy, Applied Physics Letters **97**, 173110 (2010).
[11] L. D. Landau and E. M. Lifshitz, *Quantum Mechanics (Non-relativistic Theory)*, edited by E. M. Lifshitz and L. P. Pitaevskii, Course of Theoretical Physics, Vol. 3 (Butterworth-Heinemann, 1991).
[12] M. Ahrens, R. Merkle, B. Rahmati, and J. Maier, Physica B: Condensed Matter **393**, 239 (2007).
[13] I. Pomeranchuk and Y. Smorodinsky, J. Phys. USSR **9**, 97 (1945); Y. B. Zeldovich and V. S. Popov, Soviet Physics Uspekhi **14**, 673 (1972).
[14] E. B. Kolomeisky, J. P. Straley, and H. Zaidi, Phys. Rev. B **88**, 165428 (2013).
[15] M. M. Fogler, D. S. Novikov, and B. I. Shklovskii, Phys. Rev. B **76**, 233402 (2007); D. S. Novikov, Phys. Rev. B **76**, 245435 (2007); A. V. Shytov, M. I. Katsnelson, and L. S. Levitov, Phys. Rev. Lett **99**, 246802 (2007); V. M. Pereira, J. Nilsson, and A. H. C. Neto, Phys. Rev. Lett **99**, 166802 (2007); A. Gorsky and F. Popov, Phys. Rev. D **89**, 061702 (2014); Y. Wang, V. W. Brar, A. V. Shytov, Q. Wu, W. Regan, H.-Z. Tsai, A. Zettl, L. S. Levitov, and M. F. Crommie, Nature Physics **8**, 653 (2012).
[16] A. B. Migdal, V. S. Popov, and D. N. Voskresenskii, Sov. Phys. JETP **45**, 436 (1977).
[17] M. Itoh, R. Wang, Y. Inaguma, T. Yamaguchi, Y.-J. Shan, and T. Nakamura, Phys. Rev. Lett **82**, 3540 (1999).
[18] V. L. Ginzburg, Journal of Experimental and Theoretical Physics **15**, 1945 (1945).
[19] K. V. Reich, M. Schecter, and B. I. Shklovskii, Phys. Rev. B **91**, 115303 (2015).
[20] P. A. Fleury and J. M. Worlock, Phys. Rev. **174**, 613 (1968).
[21] J. R. S. Nascimento, I. Cho, and A. Vilenkin, Phys. Rev. D **60**, 083505 (1999).
[22] L. Onsager (private communication to G.S. Manning) (1967); G. S. Manning, J. Chem. Phys. **51**, 924 (1969).

[23] For example, in salty water, the negative linear charge density of DNA is renormalized from $\simeq -4e/l_B$ to the universal net value $-e/l_B$ due to the condensation of Na^+ ions onto the DNA surface. Here $l_B = e^2/\kappa_w k_B T \simeq 7\,\mathring{A}$ where $\kappa_w = 81$ is the dielectric constant of water and T is the room temperature.
[24] K. Ueno, S. Nakamura, H. Shimotani, A. Ohtomo, N. Kimura, T. Nojima, H. Aoki, Y. Iwasa, and M. Kawasaki, Nature Materials **7**, 855 (2008).
[25] G. Khalsa and A. H. MacDonald, Phys. Rev. B **86**, 125121 (2012).
[26] M. Stengel, Phys. Rev. Lett **106**, 136803 (2011).
[27] W.-j. Son, E. Cho, B. Lee, J. Lee, and S. Han, Phys. Rev. B **79**, 245411 (2009).
[28] S. Y. Park and A. J. Millis, Phys. Rev. B **87**, 205145 (2013).
[29] J. T. Haraldsen, P. Wölfle, and A. V. Balatsky, Phys. Rev. B **85**, 134501 (2012).